Journal of Coordination Chemistry

ISSN: (Print) (Online) Journal homepage: https://www.tandfonline.com/loi/gcoo20

A review on state of art and perspectives of Metal-Organic frameworks (MOFs) in the fight against coronavirus SARS-CoV-2

Miroslav Almáši

To cite this article: Miroslav Almáši (2021) A review on state of art and perspectives of Metal-Organic frameworks (MOFs) in the fight against coronavirus SARS-CoV-2, Journal of Coordination Chemistry, 74:13, 2111-2127, DOI: 10.1080/00958972.2021.1965130

To link to this article: https://doi.org/10.1080/00958972.2021.1965130

Published online: 13 Aug 2021.

JOURNAL OF COORDINATION CHEMISTRY
2021, VOL. 74, NO. 13, 2111–2127
https://doi.org/10.1080/00958972.2021.1965130

Taylor & Francis
Taylor & Francis Group

REVIEW

A review on state of art and perspectives of Metal-Organic frameworks (MOFs) in the fight against coronavirus SARS-CoV-2

Miroslav Almáši

Department of Inorganic Chemistry, Faculty of Science, Pavol Jozef Šafárik University, Moyzesova 11, Košice, 041 54, Slovak Republic

ABSTRACT

Metal-organic frameworks (MOFs) represent a class of hybrid inorganic-organic porous materials whose development and applications have been intensively studied. The exceptional surface area, structural variability, the richness of their crystal structures and architectures allow for engineering synergies between metal nodes, functional linkers, encapsulated substrates or nanoparticles for gas adsorption and separation, heterogeneous catalysis, ion exchange, drug delivery, energetics and many more. The present review reflects on the current global pandemic situation associated with the COVID-19 disease and summarizes the applications and perspectives of MOF materials in the fight against the coronavirus SARS-CoV-2. It is mainly focused on selected MOF compounds, their crystal structures, textural properties, possible modification and application in diagnosis and elimination of coronavirus SARS-CoV-2.

GRAPHICAL ABSTRACT

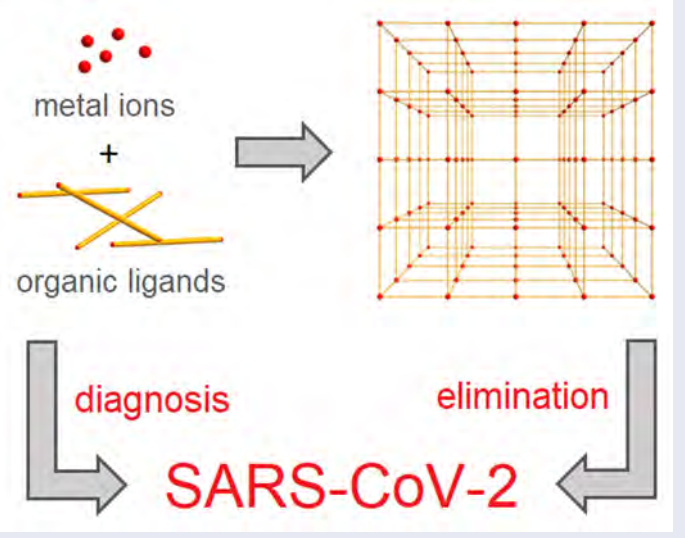

ARTICLE HISTORY
Received 6 July 2021
Accepted 3 August 2021

KEYWORDS
Metal-organic frameworks; MOF; SARS-CoV-2; COVID-19; detection; elimination

CONTACT Miroslav Almáši miroslav.almasi@upjs.sk Department of Inorganic Chemistry, Faculty of Science, Pavol Jozef Šafárik University, Moyzesova 11, 041 54 Košice, Slovak Republic

1. Introduction

Metal-organic frameworks (MOFs), also known as porous coordination polymers (PCPs), can be characterized as micro-/mesoporous hybrid inorganic–organic materials. Their inorganic part consists of metal cations or metal clusters, and the organic component is ligands, which are most often represented by carboxylic acids. These components are connected through coordination bonds to form 3 D polymeric frameworks in which pores of various dimensions and shapes are present (see Figure 1). The synthesis of MOF materials can be regarded as a construction game, which depends on the selected building blocks and their compatibility. Due to the wide choice of metal ions and the even greater choice of carboxylic acids, an infinite number of MOF compounds with different shapes and topologies of the polymeric frameworks, pore size, and surface area can be constructed [1]. Due to their extensive surface area, which reaches up to 10,000 $m^2 \cdot g^{-1}$, and the pore volumes, MOF compounds find application in various fields [2,3]. MOFs are intensively studied as gas adsorbents [4–8], gas separators [9–11], heterogeneous catalysts [12–14], ion exchangers [15,16], drug delivery systems with the sustained release [17–19], templates for nanoparticle preparation [20,21], energy storage materials [22–25] and others. For the current pandemic situation, which can be described as the greatest threat and epidemic of the 21st century, MOF materials are being studied as compounds for diagnosing and eliminating the SARS-CoV-2 virus. The present review focuses on the current state of art and perspectives of the MOF applications in the fight against coronavirus SARS-CoV-2.

2. Coronaviruses and SARS-CoV-2

Until the end of 2019, six genera of RNA viruses were known, so-called coronaviruses (CoVs), which usually cause respiratory disease in humans. So far, four of them have only occurred in a certain area of the world and have caused diseases that are slightly more severe than the common cold. However, two other genera of coronaviruses have raised global concerns, the first one causing Severe Acute Respiratory Syndrome (SARS) in 2002 and another coronavirus ten years later gave rise to Middle East Respiratory Syndrome (MERS). WHO (World Health Organization) data indicate that SARS-CoV has infected more than 8,000 people worldwide, and the mortality was approximately 10% [26]. In December 2019, a new human coronavirus appeared, which spread rapidly worldwide and has higher mortality than endemic coronaviruses, but lower than the above-mentioned SARS-CoV or MERS-CoV coronaviruses. The virus was initially named 2019-nCoV (2019 novel coronavirus), but is now called Severe Acute Respiratory Syndrome Coronavirus 2 (SARS-CoV-2) and causes COVID-19 disease (Coronavirus Disease 2019) [26]. This disease mainly affects the respiratory system and, in some cases, can cause severe pneumonia and death to the patient. At present (July 20, 2021), the infection has been confirmed in 190,671,330 people worldwide and has caused the deaths of 4,098,758 people [27], which corresponds to mortality of 2.15%. Figure 2 shows the daily development of the pandemic situation caused by COVID-19 disease from January 2020 to July 2021 (July 20, 2021), which is divided into two graphs. Figure 2a shows the daily recorded number of newly infected persons, and Figure 2b shows the daily number of deaths. As can be seen from Figure 2, the

highest boom of new confirmed cases and deaths was observed between November 2020–February 2021 and April 2021–June 2021. At present, an increasing trend in new cases is observed again, reaching a number of infected people comparable to the beginning of the second wave of the COVID-19 pandemic in April 2021. The positive news is that the overall mortality rate is lower, which can be attributed to the gradual vaccination of the population.

The enormous danger of SARS-CoV-2 lies in its rapid and inconspicuous spread. With increase in the number of cases requiring intensive care, health systems may become overwhelmed. These unfortunate statistics and prognoses call for an urgent need for more intensive research in this area of diagnosis and elimination of SARS-CoV-2 virus so that identification with the most accurate diagnostic method as well as epidemic treatment can be carried out as soon as possible.

Currently, three main routes of disease transmission are known droplets, contact and most likely also aerosol. Droplet transfer means the ingestion or inhalation of droplets excreted by an infected person during coughing, sneezing and communication by persons in their immediate vicinity. Contact transmission can occur when a healthy individual touches a virus-contaminated surface or object and then touches the mouth, nose, or eyes. Therefore, the development of surface disinfectants is necessary and desirable in order to eliminate the SARS-CoV-2 virus. Aerosol transfer can occur when the droplets mix with air to form aerosols that can be inhaled in large amounts in a relatively confined environment into the lungs and cause infection [28].

From the biochemically and structurally point of view, SARS-CoV-2 is composed of approximately 29,900 bases, which encode 16 non-structural and 4 structural proteins designed as nsp1 - nsp16, which are essential for the SARS-CoV-2 life cycle [29]. Viral RNA is protected from the innate immunity of cells by a cap that forms a specific arrangement at the 5′ end of the RNA molecule. The arrangement consists of C2′-O-methyl-ribosyladenine and N-methylated guanosine triphosphate, which resembles native host cell mRNA. In human cells, the cap is installed on newly transcribed mRNA already present in the nucleus, to which coronaviruses do not have access. Instead, SARS-CoV-2 possess their own enzymes that synthesize caps, through which they are involved in the cell cycle [30] and subsequently causes COVID-19 disease.

3. Metal-organic frameworks and SARS-CoV-2

3.1. Diagnostic of SARS-CoV-2 by MOFs

Early detection of viruses is essential for the effective prevention and treatment of associated diseases caused by the SARS-CoV-2 virus. There are currently many diagnostic techniques used to detect viruses, such as real-time polymerase chain reaction (rtPCR), quantitative polymerase chain reaction (qPCR), high-throughput sequencing, nucleic acid amplification assays, IgA antibodies and antigen testing, combined IgM-IgG, antibody testing, electrochemical sensors, etc. [31,32]. Most of these tests are expensive to manufacture, and virus detection itself is a long process. It is urgent to develop cost-effective and rapid diagnostics. In this application area, MOF-type materials should also be investigated, where they could find application in the detection of SARS-CoV-2 virus.

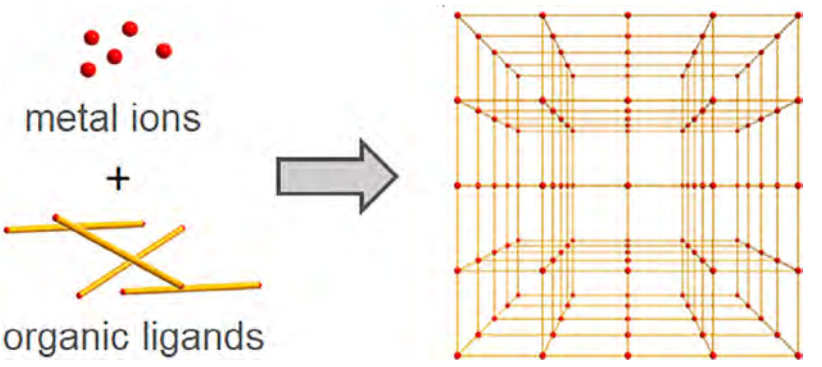

Figure 1. MOF construction using metal ions and organic linker molecules into the final 3 D polymeric open framework.

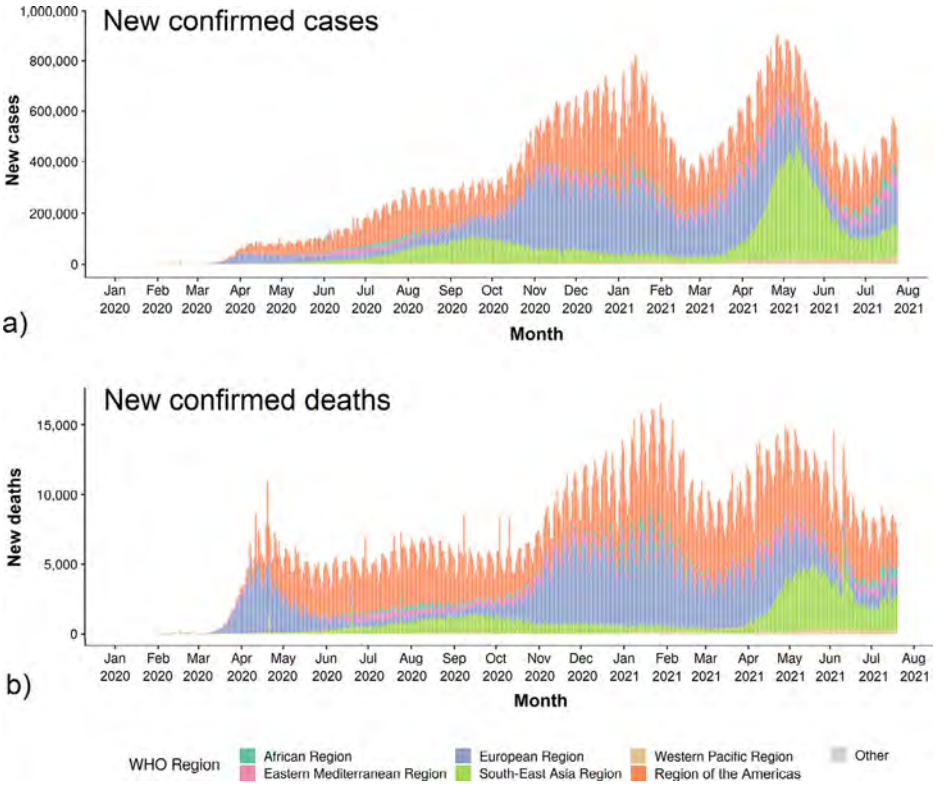

Figure 2. Development of the daily pandemic situation caused by COVID-19 disease globally from January 2020 to July 2021 divided by WHO regions. a) The number of confirmed cases and b) new confirmed deaths according to WHO [27].

Some tests for detecting viruses, including SARS-CoV-2, are based on the detection of lateral flow antigens. In general, lateral flow antigen assays are composed of a membrane on which metal nanoparticles (gold, silver, *etc.*) are anchored to which substrates can bind antibodies of the virus. Metal nanoparticles serve as the visual detection materials in which physical and chemical changes occur after virus binding, which

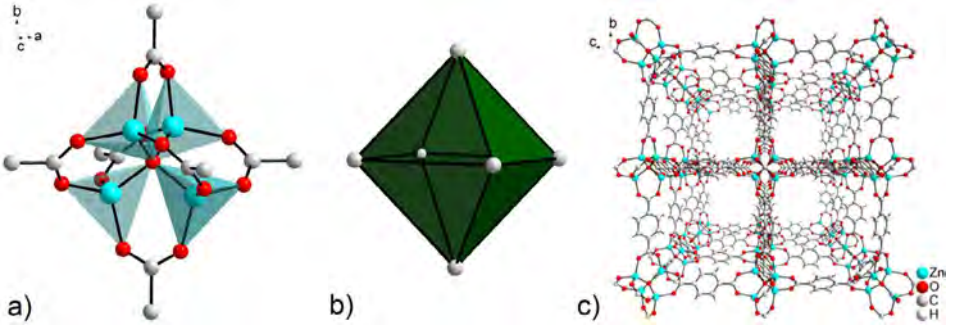

Figure 3. (a) Zn_4 (O)$(COO)_6$ cluster present in the crystal structure of MOF-5 with (b) corresponding octahedral secondary building unit and (c) final cubic polymeric framework [35].

can be detected by fluorescence and spectroscopic measurements such as CHEF (Chelation Enhanced Fluorescence) and SERS (Surface-Enhanced Raman Scattering) [33]. In this context, gold nanoparticles were mainly studied, while the detection mechanism consists of the color change caused by the binding of the virus antigen to the gold particles during the passage of the analyzed sample (urine, blood, saliva) through the membrane. The color change as optical detection of the virus depends on the type, shape, size and aggregation degree of the nanoparticles. The above described SARS-CoV-2 detection principle is mainly used in IgG and IgM tests.

An example of a possible virus detection material is MOF-5 [34]. MOF-5 is zinc terephthalate oxide with the chemical composition $[Zn_4O(BDC)_3]\cdot G$ (BDC = benzene-1,4-dicarboxylate, terephthalate; G = guest molecules) in which four zinc(II) ions share one oxide ion. In addition, Zn(II) ions are bridged by six carboxylates from BDC molecules coordinated in the *syn-syn* mode that are oriented into the corners of the octahedron (see Figure 3a). Mentioned coordination creates an electroneutral $Zn_4(O)(COO)_6$ cluster with octahedral secondary building unit (SBU, see Figure 3b), which is bridged by BDC molecules to form a cubic framework containing pores with a size of 8×8 Å propagating along all crystallographic axes (see Figure 3c). Depending on the preparation method and activation conditions, the specific surface area of MOF-5 ranged from 2,000 to 3,800 $m^2 \cdot g^{-1}$ [36,37].

Into the framework of MOF-5, gold nanorods coated with 11-mercaptoundecanoic acid (MUA) molecules have been encapsulated, and a composite material MUA-Au@MOF-5 was prepared [38]. For the increased affinity of thiol groups and gold, MUA molecules bind to the surface of gold nanorods. Carboxyl groups bond to or interact with functional groups of analytes. The described composite material was applied to detect various small organic molecules based on pyridine derivatives (pyridine, 2,6-biphenylpyridine and poly(4-vinylpyridine)), which showed high sensitivity and accuracy. Due to the presence of pyridine derivatives, different SERS activity was observed even at low analyte concentrations. The same principle could be used in the detection of SARS-CoV-2, where suitable substrates such as proteases (3CLpro [39], Nsp5 [40]), fluorogenic dipeptides [41,42], N-terminomics [43,44] or luciferase-based biosensors [45–47] would be grafted to the surface of gold nanoparticles. The substances will interact with the SARS-CoV-2 membrane, immobilize it, and subsequently be

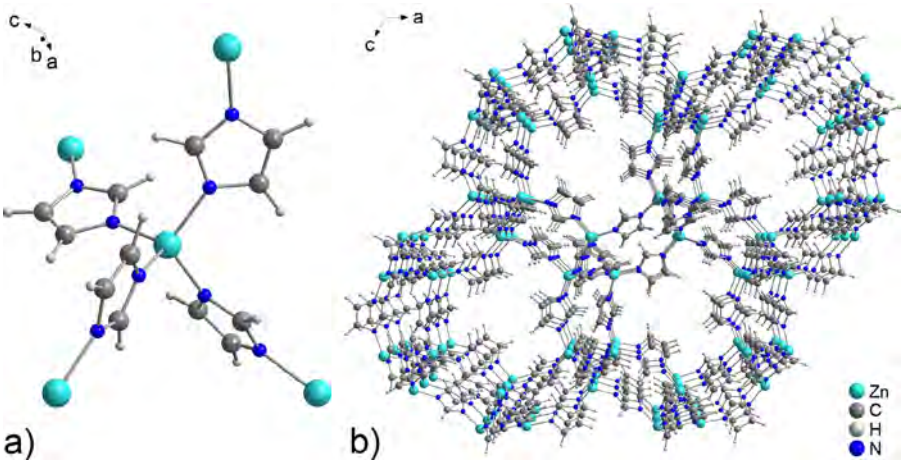

Figure 4. (a) Coordination environment of Zn(II) ions in ZIF-8 and the coordination mode of imidazolate linkers. (b) A view of the final ZIF-8 polymeric framework containing spherical cages [55].

detected by optical methods, such as fluorescence resonance energy transfer (FRET) or SERS.

Other MOFs adept for the development of antigenic assays in which stored gold nanoparticles would serve as substrates for immobilization and detection of SARS-CoV-2 are MIL-101 [48], MOF-199 [49], MOF-74 [50], IRMOF-3 [51], NU-1000 [52] and ZIF-8 [53]. Because these MOFs have been studied as materials for the preparation of Au nanoparticles. The MOF@Au composite materials thus prepared were applied as gas adsorbents, heterogeneous catalysts, or materials for the detection of small organic molecules or biomolecules [48–53]. Therefore, these compounds are suitable for further post-synthetic modification with coronavirus detection substrates.

Another material for possible coronavirus detection is ZIF-8, which belongs to the group of zeolitic-imidazolate frameworks (ZIFs) [54]. The geometric arrangement of building components and the final framework of ZIF compounds imitate well-known inorganic porous materials, zeolites. The crystal structure of ZIF-8 consists of zinc(II) ions, on which the four imidazolate molecules are tetrahedrally coordinated via nitrogen donors (see Figure 4a). The described coordination of the building components creates cages with a pore size of 14.3×14.3 Å (see Figure 4b) with inlet apertures of 4.1×4.1 Å and a surface area of $\sim$1,500 $m^2 \cdot g^{-1}$ [56].

A simple self-template strategy was proposed for preparation of semiconductors based on metal oxide@ZIF-8 core-shell heterostructures with different morphology. ZnO@ZIF-8 materials were prepared in the form of freestanding/vertically standing nanorods or 2 D layers. In the synthetic procedure, zinc(II) oxide nanorods act as the template and also a source of Zn(II) ions for ZIF-8 formation [57]. The prepared ZnO@ZIF-8 material displays a significant photoelectrochemical response to whole scavengers with inorganic and organic molecules of different sizes, ascorbic acid and hydrogen peroxide, owing to the small ZIF-8 shell's aperture. ZnO@ZIF-8 nanorods were investigated for mentioned analytes detection in saline solution representing simulated body fluid. This feature of ZnO@ZIF-8 can be used for the early diagnosis and detection of various pathogens. For this purpose, it is possible to incorporate

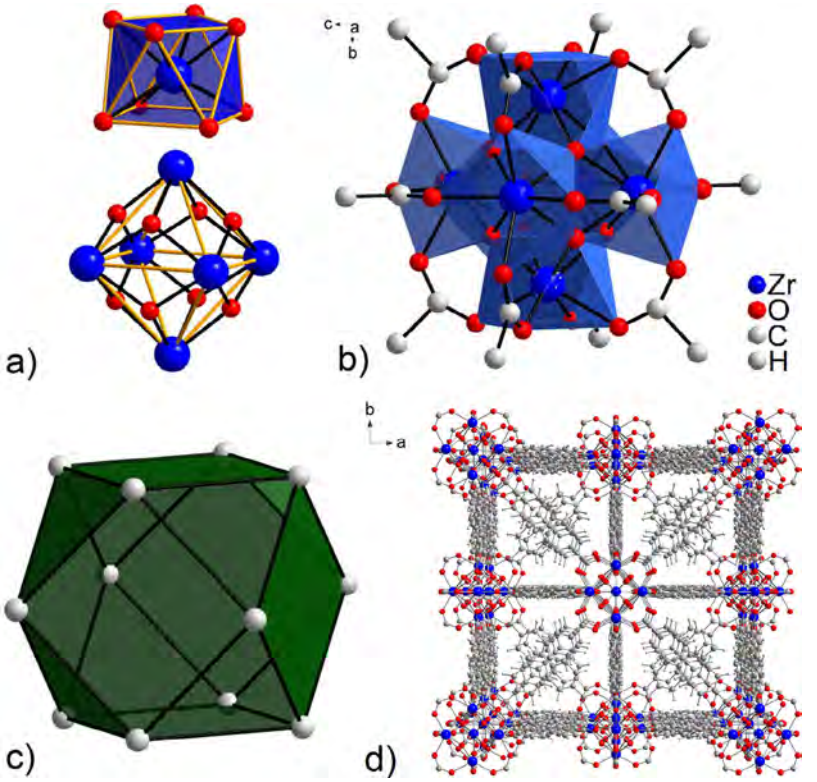

Figure 5. (a) Polyhedron with the shape of a tetragonal antiprism (top) and the octahedral arrangement of Zr(IV) ions (bottom) found in UiO-67 and UiO-66. (b) A view of the $[Zr_6(O)_4(COO)_6]$ cluster and (c) the resulting cuboctahedral shape of the secondary building unit. d) Final polymeric framework of UiO-67 built up Zr(IV) ions and BPDC building blocks [68].

different molecules with visual detection into the porous structure of MOF materials or modify their surface. By creating such a conjugated system with surface-modified suitable stimulus-responsive molecules, the resulting material can serve as a switch-on/switch-off biosensor [58–60]. The described studies show that semiconductor@MOF materials have potentially promising applications in electronic devices, including sensors for detecting SARS-CoV-2 coronavirus. Specific examples of semiconductors that were investigated for coronavirus detection are Nb_2C and Ta_2C [61]. Due to their semiconductor properties, these compounds have been shown to significantly increase the signal in the detection of SARS-CoV-2 by SERS. Nb_2C and Ta_2C exhibit a remarkable SERS enhancement with optimized SERS sensitivity in μM concentration of SARS-CoV-2 ($3.0 \times 10^6 - 1.4 \times 10^6$ M) in the analyte. Moreover, Ta_2C detection limit is possible to reduce to the concentration of *n*M (5×10^{-9} M), which is beneficial to achieve real-time monitoring and early detection of novel variants of coronavirus. Other semiconductor materials are carbon nanotubes (CNTs) which have been anchored to the gold surface [62] and also show high sensitivity in SARS-CoV-2 detection (LOD = 800 nM). Since gold is a precious metal, it would be more convenient to disperse the CNTs in porous materials, such as MOFs, and thus reduce the economic costs associated with preparing the final material.

At present, MOF materials with semiconductor@MOF composition $BiVO_4$@Au@UiO-66-NH_2 [63], TiO_2 or ZnO@MOF-5 [64], TiO_2@HKUST-1 [65], In_2S_3@MIL-68 [66] and CdS@MIL-125(Ti)-NH_2 [66] have been prepared and studied, which are perspective materials for coronavirus detection by hole scavengers.

Studies on the adsorption behavior of corona protein and cell interactions were studied using MOFs, UiO-66 and UiO-67 [67]. A common feature of both compounds is the presence of zirconium(IV) ions in their crystal structure and, for the first time, were prepared at the University of Oslo (UiO), Norway. Compounds UiO-66 and UiO-67 [67] contain $[Zr_6(O)_4(OH)_4(COO)_6]$ cluster in their crystal structures, which consists of six zirconium(IV) ions bridged by oxido, hydroxido and carboxylate ligands. Each central zirconium is eight-coordinate with oxygen ions, with a tetragonal antiprism polyhedron (see Figure 5a top). The bottom of the antiprism is formed by four oxido or hydroxido ligands and the top of the antiprism is formed by four oxygen ions of carboxylate ligands. The six zirconium(IV) cations occupy the vertices of the octahedron, and the central ions are bridged to each other by the four oxido and four hydroxido ligands forming the μ_3-bridges which are located above each wall of the octahedron (see Figure 5a). In addition, the Zr(IV) ions are bridged by twelve carboxylate groups coordinated in the *syn-syn* fashion derived from twelve different terephthalate (BDC) ligands in UiO-66 and biphenyl-4,4′-dicarboxylate (BPDC) molecules in UiO-67 (see Figure 5d), which are coordinated at each edge of the Zr_6 octahedron. The result of the described coordination is an electroneutral cluster with composition $[Zr_6(O)_4(OH)_4(COO)_6]$ (see Figure 5b) and cuboctahedron secondary building unit (see Figure 5c). Different lengths of the linkers used in the preparation of UiO materials result in different pore sizes and specific surface areas: 8×8 Å, 11×11 Å and $\sim$1,200 $m^2 \cdot g^{-1}$ for UiO-66, 12×12 Å, 16×16 Å and $\sim$3,000 $m^2 \cdot g^{-1}$ for UiO-67 [67].

MOFs have attracted considerable attention for bio-applications as drug delivery systems (DDSs) with sustained or site-specific drug release [17–19, 69]. The interactions of MOF particles with biomacromolecules in physiological systems are also currently being intensively studied to develop biorecognition devices [70–72]. As nanoparticles (NPs) enter the physiological system, some biomacromolecules attach to NP surfaces and form a protein corona due to their increased affinity and thermodynamically favorable manner [73]. In this field, UiO-66 and UiO-67 have been investigated as substrates for protein corona formation and the conformational changes in the protein itself based on MOF morphology [74]. Human albumin serum (HAS) was chosen as the model protein for this study. Because the compounds have different texture properties (pore size, specific surface area) due to the different sizes of the linkers in the frameworks, this played an essential role in HAS adsorption. The shape of the prepared nanoparticles also played a crucial role in the conformational changes of HAS. UiO-67 forms octahedral-shaped particles, and UiO-66 forms spherical particles. Both materials have a nanoparticle size of approximately 200 nm. The octahedral shape of nanoparticles has been shown to allow the facile formation of a protein monolayer on the surface of UiO-67. Moreover, UiO-67 was shown to have higher binding constants to HAS, allowing the material to store more protein than UiO-66. UiO-67 also caused considerable conformational changes that led to the transformation of HAS to corona structure. As UiO-67 has a high affinity for corona proteins, it is ideal for the immobilization of SARS-CoV-2 with its subsequent detection.

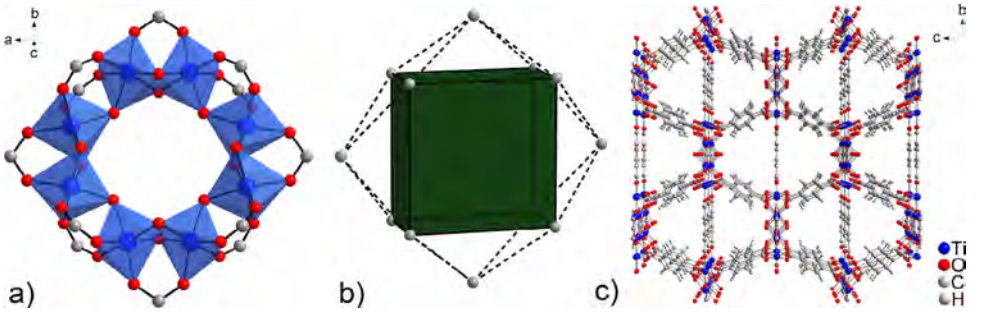

Figure 6. (a) Cyclooctanuclear cluster of Ti(IV) ions in MIL-125(Ti)-NH_2 with the corresponding (b) tetracapped tetragonal SBU and (c) final 3 D polymeric framework [88].

Similar properties can be achieved with other MOF materials that form octahedral nanocrystals of similar sizes, such as HKUST-1 (200 nm, 520 $m^2 \cdot g^{-1}$) [75], UiO-66-NH_2 (200 nm, 780 $m^2 \cdot g^{-1}$) [76], MIL-101(Cr) (200 nm, 4000 $m^2 \cdot g^{-1}$) [77,78], Fe(III)-MOF-5 (200 nm, 100 $m^2 \cdot g^{-1}$) [79,80] and UL1MOF-6 (100-200 nm, 1630 $m^2 \cdot g^{-1}$) [81].

3.2. Elimination of SARS-CoV-2 by MOFs

The coronavirus is transmitted mainly through respiratory droplets and aerosols when sneezing, coughing, or contacting other people nearby. The droplets can be inhaled or fall on a surface with which other people contact and become infected by touching their nose, mouth or eyes. Therefore, the development of disinfectants is necessary in order to eliminate the SARS-CoV-2 virus.

Some metal-organic frameworks exposed to light behave as semiconductors, making them ideal candidates for photoinduced catalysis and light-harvesting [82–84]. This created a subfield of research to fine-tune the optical response of MOF by modifying the organic linker or the inorganic unit [82,83]. In this context, highly porous titanium(IV)-based MOFs MIL-125(Ti)-NH_2 [85, 86], MIL-177(Ti) [85] and biocompatible and highly stable MIL-127(Fe) [86,87] (MIL = Materials of Institut Lavoisier, France) proved to be attractive candidates, which were tested as materials for SARS-CoV-2 elimination driven by UV irradiation.

The crystal structure of MIL-125(Ti)-NH_2 is composed of eight Ti(IV) ions that are octahedrally coordinated by six oxygen ions derived from oxido, hydroxido and 2-aminoterephthalate ligands. The central metal ions are arranged to form a cyclooctanuclear cluster with the composition $[Ti_8(O_8)(OH)_4(COO)_{12}]$ (see Figure 6a) in which the pairs of octahedra share two oxygen ions (μ_2-O) and are further bridged by one oxygen (μ_2-OH) on the inside of the cyclic cluster. On the outer side of the cluster, carboxylate ligands are coordinated in a *syn-syn* mode to Ti(IV) ions, forming a secondary building unit in the shape of a tetracapped tetragonal prism (see Figure 6b). The tetragonal prism is formed by four pairs of COO^- groups coordinated on top of each other and the capes of SBU form separate carboxylate groups as shown in Figure 6a and 6b. The coordination of building components results in a final 3 D polymeric framework (see Figure 6c), which contains octahedral and tetragonal cages of sizes 6.1 × 6.1 and 12.5 × 12.5 Å with access through micropores with a size of 5–7 Å. The

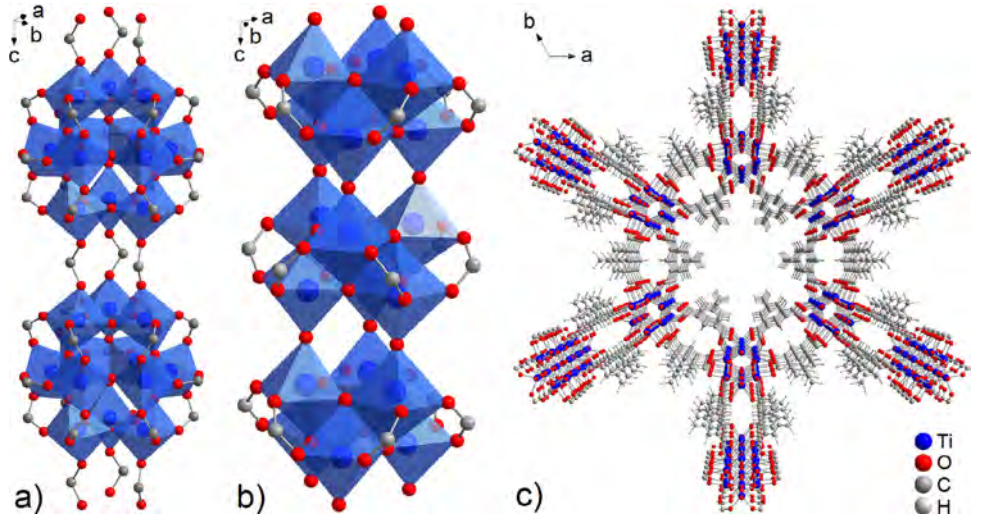

Figure 7. (a) The arrangement of Ti(IV) ions in a) MIL-177 (LT) and (b) MIL-177 (HT). (c) A view of the resulting honeycomb framework in MIL-177 (HT) [85].

specific surface area of MIL-125(Ti)-NH_2 is $\sim$ 1,600 $m^2 \cdot g^{-1}$ based on the results of nitrogen adsorption measurements [89].

MIL-177, also referred to as MIP-250 (Materials from the Institute of Porous Materials of Paris, France), belongs to the MOF family containing Ti(IV) ions, which exist in two forms, low temperature (LT) and high temperature (HT) [85]. Both forms are formed by the linker 3,3′,5,5′-tetracarboxydiphenylmethane (mdip), but differ in the arrangement of the central ions. In the crystal structure of the low-temperature form, isolated $Ti_{12}(O)_6(OH)_9(COO)_{18}$ clusters (see Figure 7a) are present, while in the MIL-177 (HT) structure, Ti(IV) ions are arranged in 1 D chains in which $Ti_6(O)_6(OH)_6(COO)_6$ subunits are connected by OH ligands (see Figure 7b). The condensation ratio (Ti(IV)/oxo ratio) plays an essential role in photocatalysis, and the mentioned ratios in MIL-177 (LT) and MIL-177 (HT) are 1.25 and 1.5, respectively. In both compounds, 1 D hexagonal channels propagating along the *c*-axis are present with a pore size of $\sim$11 Å for MIL-177 (LT) and $\sim$9 Å for MIL-177 (HT). Ti(IV) ions/clusters are located in the corners of the honeycomb framework (see Figure 7c), and the surface areas are 730 $m^2 \cdot g^{-1}$ for MIL-177 (LT) and 690 $m^2 \cdot g^{-1}$ for MIL-177 (HT).

In the crystal structure of MIL-127(Fe) [86], also referred to as PCN-250 (Porous Coordination Network) [87], three octahedrally coordinated central iron(III) cations are present, forming a $[Fe_3(O)(COO)_6(H_2O)_3]$ cluster (see Figure 8a). Each Fe(III) shares a common oxygen ion (μ_3-O) in the axial positions. The equatorial plane of each octahedron is built up of four oxygen ions of four different carboxylate groups coordinated in a *syn-syn* mode, and the last coordination position is occupied by the terminal aqua ligand (see Figure 8a). A trigonal prism-shaped secondary building block is formed from a link between the carbonyl carbon of the coordinated carboxylate groups (see Figure 8b). SBUs are connected in the crystal structure of MIL-127(Fe) via 3,3,5,5′-azobenzenetetracarboxylate (ABTC) linkers, which form the resulting polymeric framework with a specific surface area of $\sim$1,400 $m^2 \cdot g^{-1}$ containing two types of pores. 1 D

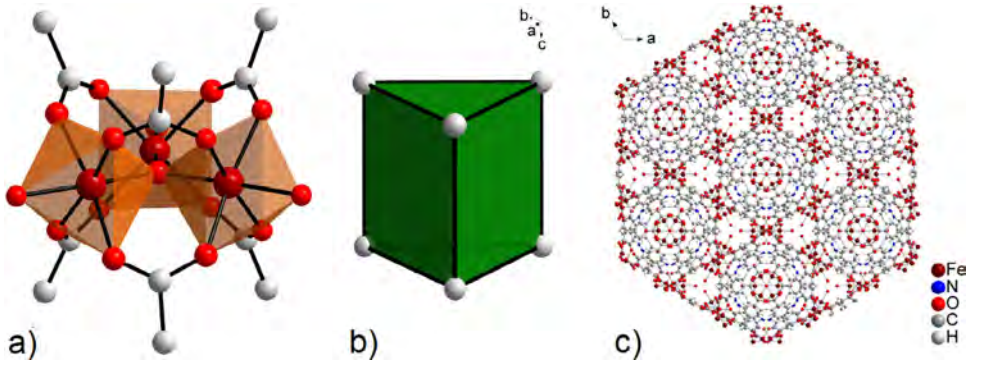

Figure 8. A view of (a) $[Fe_3(O)(COO)_6(H_2O)_3]$ cluster and (b) the corresponding trigonal prismatic SBU in MIL-127(Fe). (c) Final crystal packing of building blocks, Fe(III) ions and ABTC linkers in MIL-127(Fe) framework [87].

channels with a size of $\sim 6 \times 6$ Å and cages of 10 Å diameter with small narrow apertures of $\sim 3 \times 3$ Å [86].

Previous studies have shown that MIL-125(Ti)-NH_2 has a high affinity for water molecules and the ability to dehumidify the environment [90]. Moreover, Ti(IV) octahedra in SBU of MIL-125(Ti)-NH_2 are photochromic, which is related to the reduction of Ti(IV) to Ti(III) under UV irradiation. Studies of bandgap measurements, which generally characterize the semiconductor character of materials, have shown that the amine group in MIL-125(Ti) materials significantly reduces the bandgap value. The MIL-125(Ti) material synthesized with terephthalate (BDC) has an optical gap of 3.6 eV in the UV region (345 nm) [89]. In MIL-125(Ti)-NH_2, which contains 4-aminoterephthalate, the bandgap value is reduced to 2.6 eV and falls in the visible region (475 nm) [91,92]. The material MIL-177 (HT), which also contains photoactive Ti(IV) ions in its structure, has similar properties. Moreover, the honeycomb framework of MOF-177 (HT) is chemically stable under extremely acidic conditions, including concentrated HCl (37%), HNO_3 (65%), H_2SO_4 (98%), H_3PO_4 (6 M), aqua regia and also display strongly enhanced photoresponsive ability. The mentioned properties of MIL-125(Ti)-NH_2 and MIL-177 (HT) predetermine the materials to inactivate the SARS-CoV-2 virus using UV irradiation. MIL-127(Fe) has been studied primarily as a sustained release drug carrier [93,94], and its biocompatibility has also been confirmed. This property allows the use of this compound in the elimination of the virus on biological materials, not only surfaces of objects.

UV-C light in combination with Ti(IV) MOF produces a strong oxidative effect and may therefore be used as a photocatalytic disinfectant. Based on previous studies, it has been shown that photocatalytic elimination of the virus and subsequent development of COVID-19 disease occurs due to lipid membrane damage, RNA damage, or morphological alteration of recognition proteins on the virus surface [95,96]. Upon exposure to UV-C light, the Ti(IV)-MOF materials generate active oxygen species, superoxide ($O_2^{\cdot -}$) and hydroxyl ($^{\cdot}OH$) radicals from dioxygen and physisorbed water molecules which have high oxidative activity and decapitate the caps of the virus. The caps are an essential part of the virus through which it enters cells and engages in the cell cycle.

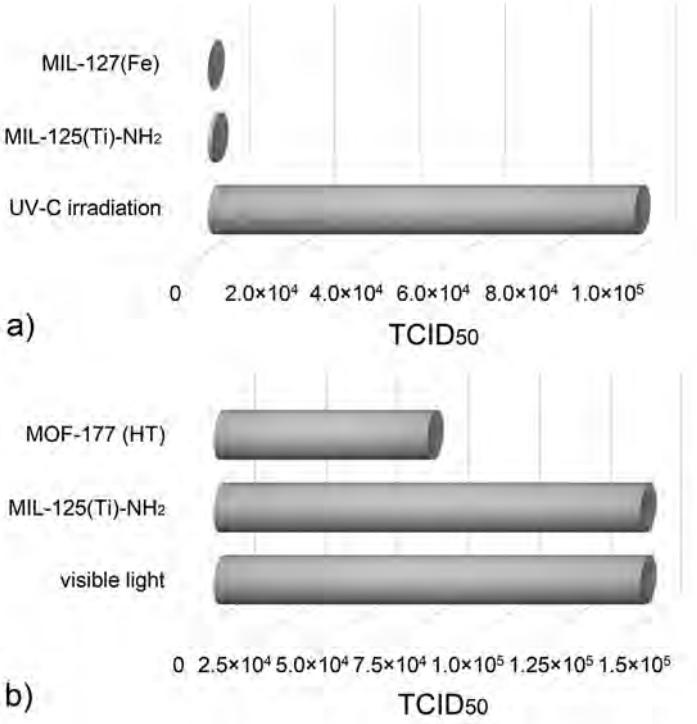

Figure 9. (a) A comparison of SARS-CoV-2 elimination by UV-C irradiation, MIL-127(Fe) and MIL-125(Ti). (b) Coronavirus inactivation by visible light, MIL-125-NH_2 and MOF-177 (HT) [102].

The nanoparticles of all three above-described MOFs were exposed to SARS-CoV-2 culture (cultivated SARS-CoV-2 virus (BEI_USA-WA1/2020)) and irradiated by UV-C light for 0.5 h. UV-C radiation is commonly used to disinfect the air, water and surfaces in the healthcare and food industry [97–101]. After exposure, the virus content in samples was analyzed by remaining viral titer by $TCID_{50}$ and RT-PCR (Reverse Transcriptase Polymerase Chain Reaction) analysis. Based on RT-PCR results, the presence of viral RNA was determined, and $TCID_{50}$ measurements estimated the elimination of SARS-CoV-2. The results showed that although the initial reduction in RNA was similar for MIL-125(Ti)-NH_2 and MIL-127(Fe), higher virus inactivation was observed using titanium(IV) MOF. For MIL-127(Fe) and MIL-125(Ti)-NH_2, a decrease in $TCID_{50}$ values from 1×10^5 (control) to 1×10^3 and 1×10^2, respectively, was observed, corresponding to 90 and 99% efficiency (see Figure 9a). As can be seen from Figure 9a, the presence of MOF materials significantly increases the amount of coronavirus eliminated compared to using UV-C radiation itself. Due to the presence of photoactive Ti(IV) ions in the structure of MIL-125(Ti)-NH_2 and low bandgap, the increased activity of the compound in eliminating SARS-CoV-2 virus could be explained [102].

Interesting results were also obtained in the inactivation of coronavirus by irradiation with visible light for 0.5 h, using MIL-125(Ti)-NH_2 and MIL-177 (HT) compounds. The advantage of this experiment is that visible light is not harmful to living organisms compared to UV-C radiation. This experiment showed that for MIL-125(Ti)-NH_2

and a control measurement without MOF material, the same $TCID_{50}$ values of approximately 1.5×10^5 were obtained, indicating the material's inability to eliminate the material SARS-CoV-2 virus by visible radiation. However, interesting results were obtained for MOF-177 (HT), when the $TCID_{50}$ value decreased to 7.5×10^3 and corresponded to 50% efficiency (see Figure 9b). The increased antiviral activity can be explained by the increased content of Ti(IV) ions (high condensation degree (oxo/Ti ratio) is 1.5), which are arranged in 1 D chains located in the hexagonal vertices of the honeycomb framework. The advantage of this material is that by its application to the object's surface (for example using a sprayer), it gradually destroys SARS-CoV-2 by the action of "ordinary" visible light and has a significant predisposition to practical use. The materials described above can be commercially purchased under the trademarks AYRSORB^{TM}-T125 (MIL-125(Ti)-NH_2) and AYRSORB^{TM}-F250 (MIL-127 (Fe), PCN-250) [103].

It has been proven that the high degree of condensation in Ti(IV)-MOF materials [104] increases their activity and selectivity in heterogeneous catalytic reactions [105] and increased adsorption capacity/selectivity in gas storage and separation [106]. They also display higher proton conductivity [107,108], which is important, especially for the development of new and efficient fuel cells and improve the signal/background noise ratio in the detection of small molecules and for this reason are suitable as sensing materials [109].

Other Ti(IV)-MOF materials [110] having a high condensation degree and promising compounds for the elimination of SARS-CoV-2 are COK-69 ($Ti_3O_3(COO)_3$, condensation degree 1.0) [111], MOF-901 ($520\,m^2 \cdot g^{-1}$, $Ti_6O_6(OCH_3)(COO)_3$, condensation degree 1.5) [107] and MOF-902 ($400\,m^2 \cdot g^{-1}$,$Ti_6O_6(OCH_3)(COO)_3$, condensation degree 1.5) [112].

4. Conclusion

MOF materials find a variety of applications in practical and industrial areas. A new topic so far less explored is the use of metal-organic frameworks to diagnose and eliminate SARS-CoV-2 coronavirus. The current review points to the potential use of MOF compounds in the diagnosis of coronavirus using encapsulated surface-modified nanoparticles for IgG and IgM assays. Other potential materials are semiconductor@MOF, which are capable of photoelectrochemical response in the interaction of analyte molecules through the hole scavengers. Based on this property, these materials can be used as sensors to detect SARS-CoV-2. Another interesting and experimentally investigated application is the use of MOF in the elimination/inactivation of coronavirus SARS-CoV-2. Prospective materials are photoactive compounds containing Ti(IV) ions with a high degree of condensation (Ti(IV)/oxo ratio). MIL-125(Ti)-NH_2, due to the low bandgap value and the presence of Ti(IV) ions, is able to eliminate 99% of the SARS-CoV-2 virus with UV-C radiation. For the high degree of condensation, MIL-177 (HT) can eliminate the virus with 50% efficiency even when exposed to visible light. These results may serve as motivation for scientific groups to study MOF materials with a high degree of condensation in the elimination of coronavirus SARS-CoV-2.

Note

All figures of crystal structures presented in this review were drawn using Diamond software [113] based on published CIF files, graphs using the Origin program [114] and corresponding sources are listed in the references.

Disclosure statement

No potential conflict of interest was reported by the authors.

Funding

This work was supported by the Development Operational Programme Integrated Infrastructure for the project "Nanoparticles for solving diagnostic-therapeutic problems with COVID-19 (NANOVIR)", ITMS 2014+:313011AUW7, co-founded by the European Regional Development Fund (ERDF).

References

[1] L. Chen, X. Zhang, X. Cheng, Z. Xie, Q. Kuang, L. Zheng. *Nanoscale Adv.*, **2**, 2628 (2020).
[2] H. Furukawa, N. Ko, Y.B. Go, N. Aratani, S.B. Choi, E. Choi, A.O. Yazaydin, R.Q. Snurr, M. O'Keeffe, J. Kim, O.M. Yaghi. *Science*, **329**, 424 (2010).
[3] R. Grünker, V. Bon, P. Müller, U. Stoeck, S. Krause, U. Mueller, I. Senkovska, S. Kaskel. Chem Commun (Camb)*)*, **50**, 3450 (2014).
[4] T. Ghanbari, F. Abnisa, W.M.A. Wan Daud. Sci Total Environ, **707**, 135090 (2020).
[5] Z. Li, P. Liu, C. Ou, X. Dong. *ACS Sustainable Chem. Eng.*, **8**, 15378 (2020).
[6] M. Almáši, V. Zeleňák, R. Gyepes, Ľ. Zauška, S. Bourrelly. *RSC Adv.*, **10**, 32323 (2020).
[7] A. Garg, M. Almáši, D.R. Paul, E. Poonia, J.R. Luthra, A. Sharma. *Front. Energy Res.*, **8**, 604735 (2021).
[8] M. Almáši, N. Király, V. Zeleňák, M. Vilková, S. Bourrelly. *RSC Adv.*, **11**, 20137 (2021).
[9] Q. Qian, P.A. Asinger, M.J. Lee, G. Han, K. Mizrahi Rodriguez, S. Lin, F.M. Benedetti, A.X. Wu, W.S. Chi, Z.P. Smith. *Chem. Rev.*, **120**, 8161 (2020).
[10] Z. Wang, Y. Tian, W. Fang, B.B. Shrestha, M. Huang, J. Jin. *ACS Appl Mater Interfaces*, **13**, 3166 (2021).
[11] M. Almáši, V. Zeleňák, R. Gyepes, S. Bourrelly, M.V. Opanasenko, P.L. Llewellyn, J. Čejka. *Inorg. Chem.*, **57**, 1774 (2018).
[12] H. Konnerth, B.M. Matsagar, S.S. Chen, M.H.G. Prechtl, F.-K. Shieh, K.C.-W. Wu. *Coord. Chem. Rev.*, **416**, 213319 (2020).
[13] T.A. Goetjen, J. Liu, Y. Wu, J. Sui, X. Zhang, J.T. Hupp, O.K. Farha. *Chem. Commun. (Camb)*), **56**, 10409 (2020).
[14] M. Almáši, V. Zeleňák, M. Opanasenko, J. Čejka. *Catal. Lett.*, **148**, 2263 (2018).
[15] C. Wang, G. Lin, J. Zhao, S. Wang, L. Zhang, Y. Xi, X. Li, Y. Ying. *Chem. Eng. J.*, **380**, 122511 (2020).
[16] M. Almáši, A. Sharma, T. Zelenka. *Inorg. Chim. Acta*, **526**, 120505 (2021).
[17] J. Cao, X. Li, H. Tian. *Curr. Med. Chem.*, **27**, 5949 (2020).
[18] H.D. Lawson, S.P. Walton, C. Chan. *ACS Appl. Mater. Interfaces*, **13**, 7004 (2021).
[19] M. Almáši, V. Zeleňák, P. Palotai, E. Beňová, A. Zeleňáková. *Inorg. Chem. Commun.*, **93**, 115 (2018).
[20] J. Yu, C. Mu, B. Yan, X. Qin, C. Shen, H. Xue, H. Pang. *Mater. Horiz.*, **4**, 557 (2017).
[21] X. Cai, Z. Xie, D. Li, M. Kassymov, S.Q. Zang, H.L. Jiang. *Coord. Chem. Rev.*, **417**, 21336 (2020).

[22] R. Zhao, Z. Liang, R. Zou, Q. Xu. *Joule*, **2**, 2235 (2018).
[23] F. Xiao, H. Wang, T. Yao, X. Zhao, X. Yang, D.Y.W. Yu, A.L. Rogach. *ACS Appl. Mater. Interfaces*, **13**, 18010 (2021).doi:10.1021/acsami.1c02301
[24] Y.Y. Hu, R.X. Han, L. Mei, J.L. Liu, J.C. Sun, K. Yang, J.W. Zhao. *Mater. Today Energy*, **19**, 100608 (2021).
[25] D. Capková, M. Almáši, T. Kazda, O. Čech, N. Király, P. Čudek, A.S. Fedorková, C. Hornebecq. *Electrochim. Acta*, **354**, 136640 (2020).
[26] Coronavirus disease (COVID–19) Pandemic. World Health Organization 2021. Available from: https://www.who.int/.
[27] Coronavirus disease (COVID–19) Weekly Epidemiological Update and Weekly Operational Update. World Health Organization 2021. Available online at: https://worldhealthorg.shinyapps.io/covid/.
[28] S.P. Adhikari, S. Meng, Y.J. Wu, Y.P. Mao, R.X. Ye, Q.Z. Wang, C. Sun, S. Sylvia, S. Rozelle, H. Raat, H. Zhou. *Infect. Dis. Pover*, **9**, 29 (2020).
[29] A. Wu, Y. Peng, B. Huang, X. Ding, X. Wang, P. Niu, J. Meng, Z. Zhu, Z. Zhang, J. Wang, J. Sheng, L. Quan, Z. Xia, W. Tan, G. Cheng, T. Jiang. *Cell Host Microbe*, **27**, 325 (2020).
[30] P. Krafcikova, J. Silhan, R. Nencka, E. Boura. *Nat. Commun.*, **11**, 3717 (2020).
[31] Y. Wang, Y. Hu, Q. He, J. Yan, H. Xiong, N. Wen, S. Cai, D. Peng, Y. Liu, Z. Liu. *Biosens. Bioelectron.*, **169**, 112604 (2020).
[32] N. Rabiee, M. Bagherzadeh, A. Ghasemi, H. Zare, S. Ahmadi, Y. Fatahi, R. Dinarvand, M. Rabiee, S. Ramakrishna, M. Shokouhimehr, R.S. Varma. *Int. J. Mol. Sci.*, **21**, 5126 (2020).
[33] B. Sharma, R.A.I. Frontiera, E. Henry, R.P. Ringe, R.P. Van Duyne. *Mater. Today*, **15**, 16 (2012).
[34] H. Li, M. Eddaoudi, M. O'Keeffe, O.M. Yaghi. *Nature*, **402**, 276 (1999).
[35] N. Lock, Y. Wu, M. Christensen, L.J. Cameron, V.K. Peterson, A.J. Bridgeman, C.J. Kepert, B.B. Iversen. *J. Phys. Chem. C.*, **114**, 16181 (2010).
[36] S.S. Kaye, A. Dailly, O.M. Yaghi, J.R. Long. *J. Am. Chem. Soc.*, **129**, 14176 (2007).
[37] C. McKinstry, R.J. Cathcart, E.J. Cussen, A.J. Fletcher, S.V. Patwardhan, J. Sefcik. *Chem. Eng. J*, **285**, 718 (2016).
[38] K. Sugikawa, S. Nagata, Y. Furukawa, K. Kokado, K. Sada. *Chem. Mater.*, **25**, 2565 (2013).
[39] M. Miczi, M. Golda, B. Kunkli, T. Nagy, J. Tőzsér, J.A. Mótyán. *Int. J. Mol. Sci.*, **21**, 9523 (2020).
[40] J.C. Milligan, T.U. Zeisner, G. Papageorgiou, D. Joshi, C. Soudy, R. Ulferts, M. Wu, C.T. Lim, K.W. Tan, F. Weissmann, B. Canal, R. Fujisawa, T. Deegan, H. Nagaraj, G. Bineva-Todd, C. Basier, J.F. Curran, M. Howell, R. Beale, K. Labib, N. O'Reilly, J.F.X. Diffley. *Biochem. J.*, **478**, 2499 (2021).
[41] H.A. Alhadrami, A.M. Hassan, R. Chinnappan, H. Al-Hadrami, W.H. Abdulaal, E.I. Azhar, M. Zourob. *Mikrochim. Acta.*, **188**, 137 (2021).
[42] W.; Rut, K.; Groborz, L.; Zhang, X.; Sun, M.; Zmudzinski, B.; Pawlik, W.; Młynarski, R.; Hilgenfeld, M.; Drag. *Nature Chemical Biology*, **17,** 222 (2021).doi:10.1038/s41589-020-00689-z
[43] T. Koudelka, J. Boger, A. Henkel, R. Schönherr, S. Krantz, S. Fuchs, E. Rodríguez, L. Redecke, A. Tholey. *Proteomics*, **21**, 2000246 (2021).
[44] P. Kaushal, C. Lee. *J. Proteomics*, **233**, 104089 (2021).
[45] A. O'Brien, D.-Y. Chen, M. Hackbart, B.J. Close, T.E. O'Brien, M. Saeed, S.C. Baker. *Virology*, **556**, 73 (2021).
[46] Z. Yao, L. Drecun, F. Aboualizadeh, S.J. Kim, Z. Li, H. Wood, E.J. Valcourt, K. Manguiat, S. Plenderleith, L. Yip, X. Li, Z. Zhong, F.Y. Yue, T. Closas, J. Snider, J. Tomic, S.J. Drews, M.A. Drebot, A. McGeer, M. Ostrowski, S. Mubareka, J.M. Rini, S. Owen, I. Stagljar. *Nat. Commun.*, **12**, 1806 (2021).
[47] X. Xie, A.E. Muruato, X. Zhang, K.G. Lokugamage, C.R. Fontes-Garfias, J. Zou, J. Liu, P. Ren, M. Balakrishnan, T. Cihlar, C.T.K. Tseng, S. Makino, V.D. Menachery, J.P. Bilello, P.Y. Shi. *Nat. Commun.*, **11**, 5214 (2020).
[48] H. Liu, Y. Liu, Y. Li, Z. Tang, H. Jiang. *J. Phys. Chem. C*, **114**, 13362 (2010).

[49] V.V. Butova, M.V. Kirichkov, A.P. Budnyk, A.A. Guda, M.A. Soldatov, C. Lamberti, A.V. Soldatov. *Polyhedron*, **154**, 357 (2018).
[50] Y. Zhang, Y. Hu, G. Li, R. Zhang. *Microchim. Acta*, **186**, 477 (2019).
[51] C. Wang, H. Zhang, X. Jiang, B. Zhou. *Analyt. Lett.*, **52**, 2439 (2019).
[52] S. Goswami, H. Noh, L.R. Redfern, K. Otake, C.W. Kung, Y. Cui, K.W. Chapman, O.K. Farha, J.T. Hupp. *Chem. Mater.*, **31**, 1485 (2019).
[53] X. Qiao, B. Su, C. Liu, Q. Song, D. Luo, G. Mo, T. Wang. *Adv. Mater.*, **30**, 1702275 (2018).
[54] P.D. Sutrisna, E. Savitri, N.F. Himma, N. Prasetya, I.G. Wenten. *IOP Conf. Ser: Mater. Sci. Eng.*, **703**, 012045 (2019).
[55] O. Karagiaridi, M.B. Lalonde, W. Bury, A.A. Sarjeant, O.K. Farha, J.T. Hupp. *J. Am. Chem. Soc.*, **134**, 18790 (2012).
[56] V.V. Butova, A.P. Budnyk, E.A. Bulanova, C. Lamberti, A.V. Soldatov. *Solid State Sci.*, **69**, 13 (2017).
[57] W.W. Zhan, Q. Kuang, J.Z. Zhou, X.J. Kong, Z.X. Xie, L.S. Zheng. *J. Am. Chem. Soc.*, **135**, 1926 (2013).
[58] W.C.W. Chan. *ACS Nano*, **14**, 3719 (2020).
[59] Z. Tang, N. Kong, X. Zhang, Y. Liu, P. Hu, S. Mou, P. Liljeström, J. Shi, W. Tan, J.S. Kim, Y. Cao, R. Langer, K.W. Leong, O.C. Farokhzad, W. Tao. *Nat. Rev. Mater.*, **5**, 847 (2020).
[60] J. Gao, L. Quan. *Med. Sci. Monit*, **26**, e928552–1 (2020).
[61] Y. Peng, C. Lin, L. Long, T. Masaki, M. Tang, L. Yang, J. Liu, Z. Huang, Z. Li, X. Luo, J.R. Lombardi, Y. Yang. *Nanomicro Lett.*, **13**, 52 (2021).
[62] R.R.X. Lim, A. Bonanni. *Trends Analyt. Chem.*, **133**, 116081 (2020).
[63] Y. Dou, S.M. Xu, A. Zhou, H. Wang, J. Zhou, H. Yan, J.R. Li. *Green Chem. Eng*, **1**, 48 (2020).
[64] C.G. Silva, A. Corma, H. García. *J. Mater. Chem.*, **20**, 3141 (2010).
[65] M. Usman, S. Mendiratta, K.L. Lu. *Adv. Mater.*, **29**, 1605071 (2017).
[66] W. Zhan, L. Sun, X. Han. *Nanomicro. Lett.*, **11**, 1(2019).
[67] J.H. Cavka, S. Jakobsen, U. Olsbye, N. Guillou, C. Lamberti, S. Bordiga, K.P. Lillerud. *J. Am. Chem. Soc.*, **130**, 13850 (2008).
[68] N. Ko, J. Hong, S. Sung, K.E. Cordova, H.J. Park, J.K. Yang, J. Kim. *Dalton Trans.*, **44**, 2047 (2015).
[69] A. Bieniek, A.P. Terzyk, M. Wiśniewski, K. Roszek, P. Kowalczyk, L. Sarkisov, S. Keskin, K. Kaneko. *Prog. Mat. Sci.*, **117**, 100743 (2021).
[70] G. Chen, S. Huang, X. Kou, F. Zhu, G. Ouyang. *Angew. Chem.*, **132**, 14051 (2020).
[71] H. Wang, L. Han, D. Zheng, M. Yang, Y.H. Andaloussi, P. Cheng, Z. Zhang, S. Ma, M.J. Zaworotko, Y. Feng, Y. Chen. *Angew. Chem. Int. Ed. Engl.*, **59**, 6263 (2020).
[72] H. Sun, J. Li, S. Yu, J. Liu. *Nanotoday*, **35**, 100985 (2020).
[73] T. Cedervall, I. Lynch, S. Lindman, T. Berggard, E. Thulin, H. Nilsson, K.A. Dawson, S. Linse. Proc. Natl. Acad. Sci. USA, **104**, 2050 (2007).
[74] N. Gan, Q. Sun, L. Zhao, P. Tang, Z. Suo, S. Zhang, Y. Zhang, M. Zhang, W. Wang, H. Li. *Int. J. Biol. Macromol.*, **140**, 709 (2019).
[75] R. Kaur, A. Kaur, A. Umar, W.A. Anderson, S.K. Kansal. *Mat. Res. Bullet.*, **109**, 124 (2019).
[76] T. He, X. Xu, B. Ni, H. Wang, Y. Long, W. Hu, X. Wang. *Nanoscale*, **9**, 19209 (2017).
[77] B. Shen, X. Chen, K. Shen, H. Xiong, F. Wei. *Nat. Commun.*, **11**, 2692 (2020).
[78] T. Zhao, S.H. Li, L. Shen, Y. Wang, X.Y. Yang. *Inorg. Chem. Commun.*, **96**, 47 (2018).
[79] Y. Valentino, K.J. Tang, R.R. Salunkhe, X. Jiang, A. Yu, K.C.W. Wu, Y. Yamauchi. *Adv. Mater.*, **29**, 1604898 (2017).
[80] W. Yin, Y. Shen, F. Zou, X. Hu, B. Chi, Y. Huang. *ACS Appl. Mater. Interfaces*, **7**, 4947 (2015).
[81] M.H. Pham, G.T. Vuong, F.G. Fontaine, T.O. Do. *Cryst. Growth Des.*, **12**, 1008 (2012).
[82] L. Li, X.S. Wang, T.F. Liu, J. Ye. *Small Methods*, **4**, 2000486 (2020).
[83] Y. Li, Y. Fu, B. Ni, K. Ding, W. Chen, K. Wu, X. Huang, Y. Zhang. *AIP Adv.*, **8**, 035012 (2018).
[84] X. Chen, X. Peng, L. Jiang, X. Yuan, H. Yu, H. Wang, J. Zhang, Q. Xia. *Chem. Eng. J.*, **395**, 125080 (2020).

[85] S. Wang, T. Kitao, N. Guillou, M. Wahiduzzaman, C. Martineau–Corcos, F. Nouar, A. Tissot, L. Binet, N. Ramsahye, S. Devautour–Vinot, S. Kitagawa, S. Seki, Y. Tsutsui, V. Briois, N. Steunou, G. Maurin, T. Uemura, C. Serre. *Nat. Commun.*, **9**, 1660 (2018).
[86] H. Chevreau, A. Permyakova, F. Nouar, P. Fabry, C. Livage, F. Ragon, A. Garcia-Marquez, T. Devic, N. Steunou, C. Serre, P. Horcajada. *CrystEngComm.*, **18**, 4094 (2016).
[87] S. Yuan, X. Sun, J. Pang, C. Lollar, J.S. Qin, Z. Perry, E. Joseph, X. Wang, Y. Fang, M. Bosch, D. Sun, D. Liu, H.C. Zhou. *Joule*, **1**, 806 (2017).
[88] A.P. Smalley, D.G. Reid, J.C. Tan, G.O. Lloyd. *CrystEngComm.*, **15**, 9368 (2013).
[89] M. Dan–Hardi, C. Serre, T. Frot, L. Rozes, G. Maurin, C. Sanchez, G. Férey. *J. Am. Chem. Soc.*, **131**, 10857 (2009).
[90] M. Sohail, Y.N. Yun, E. Lee, S.K. Kim, K. Cho, J.N. Kim, T.W. Kim, J.H. Moon, H. Kim. *Cryst. Growth Des.*, **17**, 1208 (2017).
[91] Y. Fu, D. Sun, Y. Chen, R. Huang, Z. Ding, X. Fu, Z. Li. *Angew. Chem. Int. Ed. Engl.*, **51**, 3364 (2012).
[92] Y. Horiuchi, T. Toyao, M. Saito, K. Mochizuki, M. Iwata, H. Higashimura, M. Anpo, M. Matsuoka. *J. Phys. Chem. C*, **116**, 20848 (2012).
[93] S. Rojas, I. Colinet, D. Cunha, T. Hidalgo, F. Salles, C. Serre, N. Guillou, P. Horcajada. *ACS Omega*, **3**, 2994 (2018).
[94] I. Tibbetts, G.E. Kostakis. *Molecules*, **25**, 1291 (2020).
[95] D. Gerrity, H. Ryu, J. Crittenden, M. Abbaszadegan. *J. Environ. Sci. Health A: Tox. Hazard. Subst. Environ. Eng.*, **43**, 1261 (2008).
[96] R. Nakano, H. Ishiguro, Y. Yao, J. Kajioka, A. Fujishima, K. Sunada, M. Minoshima, K. Hashimoto, Y. Kubota. *Photochem. Photobiol. Sci*, **8**, 1293 (2012).
[97] R.C. She, D. Chen, P. Pak, D.K. Armani, A. Schubert, A.M. Armani. *Biomed. Opt. Express.* , **11**, 4326 (2020).
[98] S. Cremers-Pijpers, C. van Rossum, M. Dautzenberg, H. Wertheim, A. Tostmann, J. Hopman. *Infect. Prevent. Pract.*, **3**, 100133 (2021).
[99] C.E. Ochoa-Velasco, R. Ávila-Sosa, P. Hernández-Carranza, H. Ruíz-Espinosa, I.I. Ruiz-López, II, J.A. Guerrero-Beltrán. *Food Eng. Rev.*, **12**, 290(2020).
[100] O.J. Esua, N.L. Chin, Y.A. Yusof, R. Sukor. *Processes*, **8**, 1433 (2020).
[101] C.C.R. Ramos, J.L.A. Roque, D.B. Sarmiento, L.E.G. Suarez, J.T.P. Sunio, K.I.B. Tabungar, G.S.C. Tengco, P.C. Rio, A.L. Hilario. *Int. J. Health Sci.*, **14**, 52 (2020).
[102] J. Ornstein, R.O.K. Ozdemir, A. Boehme, F. Nouar, C. Serre, D.N. Ackerman, V.L. Herrera, J.L. Santarpia. *medRxiv* (2020). https://doi.org/10.1101/2020.10.01.20204214
[103] framergy company, Inc. of College Station, Texas, USA, 2021 Available online at: www.framergy.com/
[104] S. Wang, C. Serre, N. Gouillou, N. Steunou. 2016 High degree of condensation titanium-based inorganic-organic hybrid solid material, method for preparing same and uses thereof, European patent No. EP 3 254 755 A1.
[105] S. Yuan, T.-F. Liu, D. Feng, J. Tian, K. Wang, J. Qin, Q. Zhang, Y.-P. Chen, M. Bosch, L. Zou, S.J. Teat, S.J. Dalgarno, H.-C. Zhou. *Chem. Sci.* , **6**, 3926 (2015).
[106] Y. He, W. Zhou, G. Qian, B. Chen. *Chem. Soc. Rev.* , **43**, 5657 (2014).
[107] H.L. Nguyen, P. Gándara, H. Furukawa, T.L.H. Doan, K.E. Cordova, O.M. Yaghi. *J. Am. Chem. Soc.* , **138**, 4330 (2016).
[108] H. Wang, Q.L. Zhu, R. Zou, Q. Xu. *Chem*, **2**, 52 (2017).
[109] Z. Hu, B.J. Deibert, J. Li. *Chem. Soc. Rev.*, **43**, 5815 (2014).
[110] H. Assi, G. Mouchaham, N. Steunou, T. Devic, C. Serre. *Chem. Soc. Rev.*, **46**, 3431 (2017).
[111] C. Serre, G. Férey. *Inorg. Chem.*, **38**, 5370 (1999).
[112] H.L. Nguyen, T.T. Vu, D. Le, T.L.H. Doan, V.Q. Nguyen, N.T.S. Phan. *ACS Catal.*, **7**, 338(2017).
[113] K. Brandenburg, H. Putz. 2017 *DIAMOND–Crystal and Molecular Structure Visualization, Version* 4.5, Crystal Impact GbR, Bonn.
[114] Origin(Pro), Version *9.0*. OriginLab Corporation, Northampton, MA (2013).